Heliyon xxx (xxxx) xxx

Contents lists available at ScienceDirect

Heliyon

journal homepage: www.cell.com/heliyon

Research article

Post-movement stabilization time for the downwash region of a 6-rotor UAV for remote gas monitoring

Jacob L. Brinkman, Brent Davis, Catherine E. Johnson *

Department of Mining and Nuclear Engineering, Missouri University of Science and Technology, 226 McNutt Hall, 1400 N. Bishop Ave., Rolla, MO, 65409, USA

ARTICLE INFO

Keywords:
Gas monitoring
UAV
Downwash
Stabilization time
Remote sensing
Atmospheric science
Environmental analysis
Environmental management
Environmental pollution
Environmental science
Engineering

ABSTRACT

Unmanned aerial vehicles (UAV) have been used to monitor gas emissions for research projects, though downwash, the airflow produced by the UAV rotors, is potentially capable of artificially altering gas concentration measurements. Anemometers, placed at ten different distances below a 6-rotor UAV, measured air speeds in the downwash region. The collected data was used in combination with UAV rotor speed data to determine the stabilization time of the downwash region after the UAV has returned to a stable hovering position. The stabilization time will determine the amount of time after UAV movement until reliable concentration readings can be obtained within the downwash region. This paper presents stabilization times after vertical upward and rotational UAV movement.

1. Introduction

Multi-rotor unmanned aerial vehicles (UAV) are being used with increased frequency to carry gas monitors for measuring concentrations of gas releases. Smidl and Hofman (2013) published one of the first papers to discuss using UAVs to measure gas concentrations, though the discussion was purely theoretical. Since then, four more papers were found discussing theoretical applications of UAV-mounted gas monitors (Alvear et al., 2017; 2018; Bolla et al., 2018; Nash, 2017), and six papers were found to actually attempt data collection (Aboubakr et al., 2017; Ali et al., 2017; Barchyn et al., 2018; Chang et al., 2016, 2018; Liu et al., 2018). However, none of these papers discussed the potential measurement errors inherent with using such a system.

While in flight, the UAV creates downwash, which is a zone of air disturbance created by the UAV's rotor thrust. Downwash has the potential to create pressure changes, which can affect gas concentration measurements taken inside of the downwash region. Three published papers have been found that discussed the implementation of UAV-mounted gas monitors that attempt to bypass the downwash problem (Brady et al., 2016; McCray, 2016; Yao et al., 2018). Eight papers were found to model downwash beneath UAVs, which found the downwash region to extend downward in a conical shape to a distance up to 5 m, though the downwash region rarely exceeded 1 m horizontally from the rotors (Haas et al., 2014; Ni et al., 2017; Shukla and Narayanan, 2018; Villa et al., 2016; Yang et al., 2017, 2018; Yeo et al., 2015; Zheng et al., 2018). Seven papers were found to attempt evaluating concentration measurement errors caused by downwash (Alvarado et al., 2017; Aurell et al., 2017; Gu et al., 2018; Qing et al., 2017; Roldan et al., 2015; Villa et al., 2016; Zhou et al., 2017). While all of these papers may be useful in determining error caused by downwash, these papers assume that the UAV is hovering in a stationary position or that UAV movement does not have significant effect on downwash error.

While the UAV is hovering in a stationary position, the air velocities in the downwash region are relatively constant. In contrast, the individual rotor thrusts are changing when the UAV is in motion, which in turn will alter the downwash air velocities. Changes in air velocity will create changes in air pressure, which has the potential to alter the gas concentrations. Accounting for every possible combination of rotor thrust is not currently feasible, but error evaluation can be simplified by only considering measurements taken when the downwash region is relatively stable. In addition to the time that the aircraft is in motion, more time may be required for the downwash region to stabilize after UAV motion has ceased. This paper presents a determination of the time required after UAV movement for wind speeds in the downwash region to stabilize.

* Corresponding author.
E-mail address: johnsonce@mst.edu (C.E. Johnson).

https://doi.org/10.1016/j.heliyon.2020.e04994
Received 7 August 2019; Received in revised form 1 April 2020; Accepted 17 September 2020

2. Method

The goal for the testing in this paper is to determine the time for the air velocity under the craft to return to a constant rate after the craft has ceased maneuvering. The experimental design monitored changes to the downwash region after completing vertical motion upward and downward, horizontal motion, and rotational motion.

2.1. Equipment

The UAV studied for this project was a 6-rotor DJI Matrice 600 Pro. The UAV is shown in Figure 1, though the camera was removed for this experiment. This UAV was selected due to commercial availability, while also considering the carrying capacity, flight time, and flight speed. The flight time is expected to be 16–32 min, depending on payload weight and wind conditions. The payload capacity is 6 kg. A gas monitor is expected to weigh less than 3.5 kg, so the UAV should be capable of achieving a relatively long flight time. The UAV is also capable of moving at speeds up to 65 km/h, which allows for rapid approach to the sampling location (DJI 2018). All of the UAV's capabilities theoretically allow the UAV-gas monitor system to maximize the sampling time.

Holdpeak 866A anemometers were selected as an economical anemometer that is capable of recording results in real time. The anemometers take samples once per second, calculating a time weighted average of the wind speed measured over each second, which was also the fastest sampling anemometer that was available commercially to the authors' knowledge. Each anemometer was connected to a laptop at the test site to record wind speed data.

A stand was built to elevate the UAV so the rotors are 4.66 m above the ground. The UAV was operated in a controlled building to prevent outside wind interference. The stand was required to maintain a constant position because the building structure interfered with the UAV's Global Navigation Satellite System positioning. The tallest height at which the stand can support the UAV's weight is 4.66 m, and this height is beyond the theoretical point at which ground interference produces significant airflow backwash for a 6-rotor UAV (Zheng et al., 2018). The final version of the stand, with the UAV and anemometers in place, can be seen in Figure 2. The stand grips onto the bottom chassis of the UAV. The original plan was to create a stand that reached over the UAV so that no parts would be beneath the UAV in attempt to minimize the stand's interference with the downwash. Unfortunately, the design was predicted to be too unstable, so the final stand design does extend directly below the UAV. This experiment did not evaluate the effects of the stand on the downwash region. Despite this, the stand was successful in preventing UAV motion for any thrust combination.

2.2. Test procedure

On the stand, the UAV rotors were 4.66 m above the ground. For this test, two anemometers were placed at ten distances from 0.52 m to 3.48 m beneath the UAV rotors. Of the eighteen found papers that use a UAV-mounted gas monitor, four placed the measuring point above the UAV (Alvarado et al., 2017; Brady et al., 2016; Roldan et al., 2015; Zhou et al., 2017), three placed the measuring point horizontally from the UAV (Villa et al., 2016; 2017; 2019), and twelve placed the measuring point beneath the UAV (Aboubakr et al., 2017; Ali et al., 2017; Aurell et al., 2017; Barchyn et al., 2018; Chang et al., 2016, 2018; Gu et al., 2018; Liu et al., 2018; McCray, 2016; Neumann, 2013; Smidl and Hofman, 2013; Yao et al., 2018). Gas monitor placement beneath the UAV appears in 63% of found papers, which implies this as the most popular configuration. Of the five tests that attempted to evaluate accuracy for a UAV system, the tests with measuring points beside and above the UAV saw results similar to results measured with no downwash (Aurell et al., 2017; Villa et al., 2016), while the tests with measuring points above the UAV measured error up to 50% (Alvarado et al., 2017; Roldan et al., 2015; Zhou et al., 2017). This project focused on the downwash region beneath the UAV because of the popularity of this configuration and the potential for greater inconsistency while measuring above the UAV.

At each anemometer distance beneath the UAV, at least four iterations were performed for vertical upward and rotational UAV movement. The UAV's programming does not allow vertical downward or horizontal movement while the UAV is on the ground. While on the stand, the UAV recognizes that its height is not changing, so it believes it is on the ground, which means this experiment cannot study vertical downward or horizontal motion. For consistency, a timer was used to ensure that the operator applied the thrust for 5 s for each iteration. The timer was also used to allow at least 60 s for the downwash region to stabilize between

Figure 1. UAV used for this project (camera removed prior to testing).

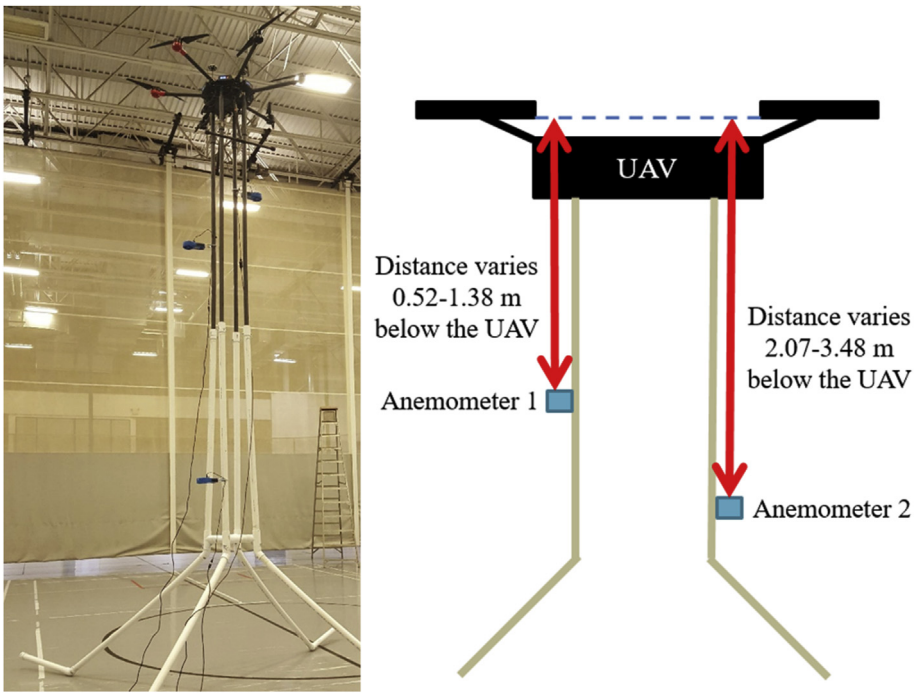

Figure 2. Final Setup with UAV, Stand, and Anemometers; Left – Actual Setup; Right – Schematic Showing Anemometer Distance (arrows) below the Bottom of the UAV rotors (dashed line).

each iteration. The anemometers were connected to the same stand as the UAV, oriented perpendicular to the stand to measure air velocity moving vertically downward. Clamps were used to extend the center of each anemometer 0.17 m from the stand post. Using multiple anemometers and distances allowed researchers to view how the air velocity behaved as the distance is increased from the UAV.

3. Results and discussion

The data collection plan is shown in Table 1. Only two anemometers were available for this test, so five separate "flights" were performed to study the ten anemometer distances. Flight 4 was interrupted by a loose anemometer clamp connection, which caused Anemometer 2 to turn perpendicular to the downwash flow direction. Data was still obtainable from readings taken prior to the clamp failure, but the test was repeated in the field as a precaution, resulting in two iterations of Flight 4 that both produced some useful data. For the remainder of Section 3, individual flight results shown are taken from Flight 4b, which is representative of all test results.

3.1. Hovering stationary

The average "hovering" rotor speed over all periods where the UAV is fully powered on and thrust is not applied was very consistent with a 1.0% or lower std. dev., shown in Table 2.

The rotor speeds are probably lower than the actual hovering rotor speeds because the stand provided support rather than the rotor thrust providing sole support, which would be the case during unrestrained flight. Therefore, while it is on the stand, the UAV system's calculations assume it is still resting on the ground where full hovering speeds are not required. Additionally, the resting speed decreases with each flight from 1532 RPM to 1415 RPM. As the battery levels decreased, the stationary speeds also decreased, which the authors believe to be a difference unique to placing the UAV on a stand. If the UAV were actually hovering, the same thrust would be required to maintain the hover position, so the thrust is relatively constant regardless of the battery level. A test flight was performed to verify this, recording 3 min of data while "hovering" on the ground, 10 min of data while hovering in air, and then 3 more min while "hovering" on the ground. Weather conditions during the flight

Table 1. Anemometer locations during test 4 flights.

	Distance Below UAV (m)		Number of Samples	
	Anemometer 1	Anemometer 2	Vertical	Rotational
Flight 1	0.52	2.07	4	5
Flight 2	0.88	2.36	8 & 6**	5
Flight 3	1.13	2.65	5	5
Flight 4a	1.38	3.08	5 & 6**	0
Flight 4b	1.38	3.08	5	5
Flight 5	1.81*	3.48	0***	5

* Data lost.
** An anemometer clamp came loose, so the two anemometers recorded a different number of samples.
*** UAV battery died prior to collecting the data. Facility time restrictions did not allow recharging or getting new batteries.

Table 2. Average "hovering" rotor speeds during test 4.

Flight Number	Anemometer Locations (m below the UAV)		Average Hover Rotor Speed (RPM)	Std. Dev.	Number of Samples
	Anemometer 1	Anemometer 2			
1	0.52	2.07	1532	0.8%	17,899
2	0.88	2.36	1487	1.0%	23,891
3	1.13	2.65	1457	0.6%	19,106
4a	1.38	3.08	1442	0.6%	10,349
4b	1.38	3.08	1428	0.7%	18,823
5	-	3.48	1415	0.5%	12,419

were 25 °C, 5 mph wind speed, and 82% humidity. The rotor speeds experienced virtually no change while hovering in the air (0% change with 0.1% std. dev.), despite the battery levels decreasing 49% during the test. However, the post-flight period of "hovering" on the ground saw rotor speeds that were over 9% lower than the pre-flight period. The results confirm that battery level does affect "hovering" rotor speed while on the ground, but the rotor speeds will not decrease during actual flight.

Table 3 shows the average air velocity during a period of at least 4 min during which the UAV thrust is not changed.

The average wind speed increases with distance from the UAV until 1.13 m, after which it decreases with distance from the UAV. The trend is consistent despite the changing UAV rotor speeds as the battery level decreases. The initial period of increasing wind speed also has considerably higher standard deviations. Papers found during the literature review discussed a conical region immediately beneath the body of the UAV that experiences relatively low air velocity and relatively high turbulence because the rotors push air vertically, not into the space immediately beneath the UAV body. The anemometers at 0.52 m and 0.88 m were likely inside that conical region, evidenced by the lower wind speeds and high standard deviations. Adding even more evidence, the researchers observed during preliminary setup that the anemometer vane rotation at 0.52 m below the UAV would periodically change directions, not shown in the results because the anemometer only records absolute values. The reverse direction phenomenon could not be replicated for video recording during subsequent testing, but the problems seen in this highly turbulent conical region make it unlikely to determine any meaningful information from the results at this distance. High turbulence means continual changes in velocity, which in turn will also change the air pressure and gas concentrations. For gas measurement, a consistent speed is more desirable in order to maintain relatively constant air pressure, which in turn relates to more reliable gas concentration results. Therefore, even though the conical region has relatively low average wind speed, the greater inconsistencies seen during this test show that this region is not ideal for gas measurement. The exact end of the conical region was not defined in this test, but it likely ends between 0.88 m and 1.13 m beneath the UAV rotors.

The trend in the wind speed standard deviations shows an ideal distance for obtaining accurate results for this UAV and stand. The deviation decreases until 2.07 m, after which it stays the same at 2.36 m before increasing again until 3.48 m. It is possible that the initially increasing stability is caused by decreasing wind speeds to a point where turbulence is minimal. The final decreasing stability may be caused by interference with the ground as air impacting the ground may be backwashed into the downwash region, though further testing will be required to verify this. For testing with this stand, a distance of 2.07–2.36 m from the rotors has the most stable wind velocity.

3.2. Rotor speed results

The six individual UAV rotor speeds over the test durations were taken from the UAV's internal record system. Flight 4b results are shown in Figure 3 as an example. The initial spike at approximately 40 s is when the rotors were turned on. Each of the remaining peaks represents changes made in the UAV thrust. The first five peaks represent the simulation of upward movement. The operator increased the thrust as if the UAV were accelerating upward, and then released the throttle to allow the UAV to return to the hovering thrust. The following five series of peaks represents rotational movement.

The graphical results for each of the six rotor speeds are visually very similar. In order to accentuate differences, Figure 4 has offset the results so each plot can be viewed individually. As shown, the results are still primarily very similar, aside from the final five peaks that pertain to rotational motion. Only the right side, left front, and left back rotors experience thrust, while the other three remain at the average hovering rotor speed. The UAV rotor arms alternate clockwise and counterclockwise rotation, and the three rotors that experience peaks are the three rotors that rotate clockwise. The operator only moved the UAV in the clockwise direction, which is why these three rotors experienced more thrust to counteract the counterclockwise rotors. Counterclockwise movement would simply have the opposite effect, so studying both directions would be redundant. These five peaks associated with rotational movement have significantly lower peak rotor speeds than observed in vertical movement. The difference in rotor speed is potentially caused by the greater kinetic energy required to change the UAV's potential energy moving vertically, rather than the rotational movement that maintains the same potential energy.

Table 3. Average "hovering" wind velocities (No UAV movement).

Distance below UAV (m)	Average Hover Wind Speed (m/s)	Std. Dev.	Number of Samples
0.52	3.01	25.4%	249
0.88	4.11	11.6%	436
1.13	4.23	7.2%	263
1.38	4.09	6.6%	303
2.07	3.96	4.4%	284
2.36	3.92	4.4%	345
2.65	3.66	5.4%	266
3.08	3.48	5.3%	306
3.48	3.21	6.2%	447

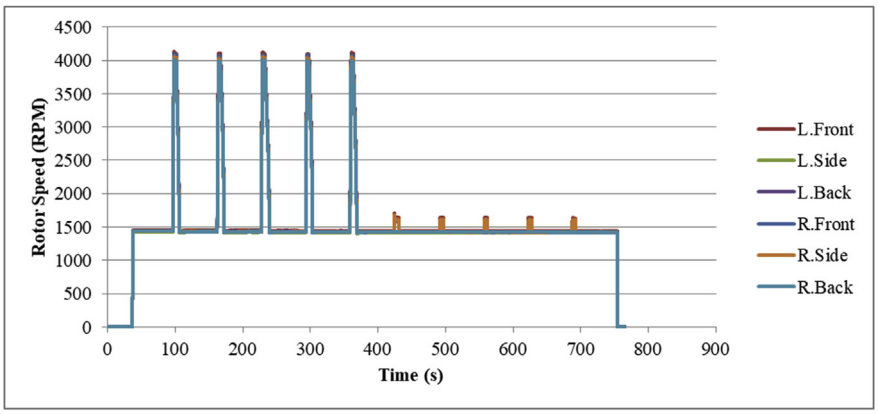

Figure 3. Flight 4b UAV rotor speed over time.

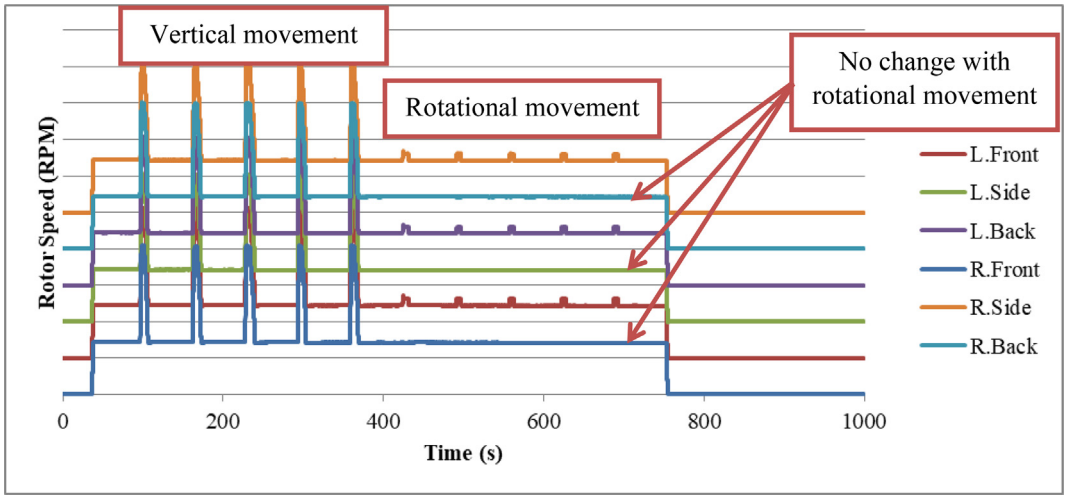

Figure 4. Flight 4b UAV rotor speed, offset to make individual rotor results more prominent.

3.3. Wind velocity results

The air velocities measured by the anemometers are shown in Figure 5, where time 0 is the same as time 0 in Figure 3 and Figure 4. The data from both anemometers has peaks that appear to align with the vertical movement peaks in Figure 3. However, it is unclear what caused the spike at approximately 250 s for the anemometer at 1.38 m. The results from the anemometer located at the greatest distance beneath the UAV experiences lower wind speeds. For example, in Figure 5, the anemometer at 3.08 m has wind speeds lower than the anemometer at 1.38 m. This trend was seen in nearly all results as previously discussed in Table 3. Lastly, the data does not visually appear to have peaks associated with rotational movement, which is likely due to the lower changes in rotor speed.

3.4. Vertical movement upward

For upward vertical movement, the operator engaged the throttle for 5 s, reaching peak rotor speeds up to 185.4% greater than the "hovering"

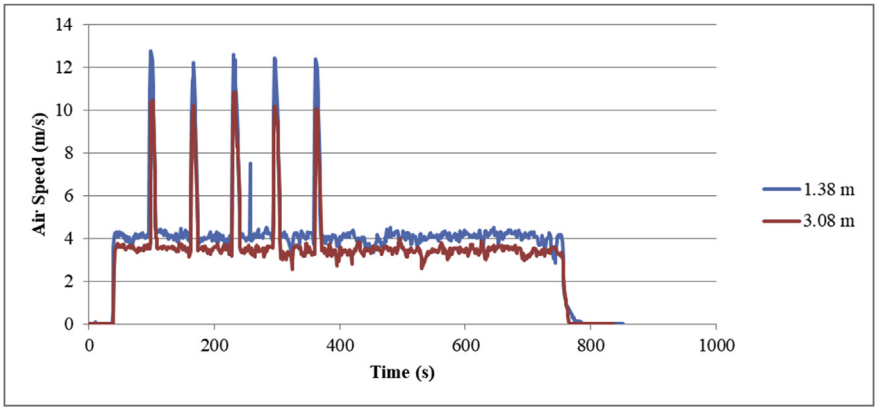

Figure 5. Test 3 air speed measurements over time.

Table 4. Results after simulating vertically upward UAV movement, flight 4b.

Anemometer Location	No.	Event Times (s)					Time Downwash Air Speed Was Disturbed (s)			Stabilization Time (s)	
		Throttle Applied	Throttle Released	Throttle Duration	Rotor Speeds Return to Hover	Time to Return to Hover	Begin	End	Total	After Releasing Throttle	After Rotor Speed Returns to Hover
1.38 m below the UAV	1	96.538	101.616	5.078	106.218	4.602	96	106	10	4	0
	2	162.194	167.336	5.142	172.540	5.204	163	173	10	6	0
	3	227.701	233.348	5.647	239.671	6.323	229	241	12	8	1
	4	293.268	298.167	4.899	303.333	5.166	294	304	10	6	1
	5	358.723	363.691	4.968	368.760	5.069	360	370	10	6	1
3.08 m below the UAV	1	96.538	101.616	5.078	106.218	4.602	98	109	11	7	3
	2	162.194	167.336	5.142	172.540	5.204	163	174	11	7	1
	3	227.701	233.348	5.647	239.671	6.323	229	241	12	8	1
	4	293.268	298.167	4.899	303.333	5.166	294	309	15	11	6
	5	358.723	363.691	4.968	368.760	5.069	361	371	10	7	2

rotor speed. The results for Flight 4b are shown in Table 4. If the air speed at any point in time had a deviation from the mean that was greater than two times the standard deviation for at least three consecutive 1-second periods, then the air speed at that time was assumed to be disturbed. For example, the air speed at the anemometer 1.38 m below the UAV had an average wind speed of 4.09 m/s with 6.6% standard deviation. Between 96 and 106 s, deviation from the mean ranged from 30.1% to 207%, coinciding with the time the UAV rotor speeds were above the mean rotor speed. Therefore, the air velocity was disturbed during that time, and the total time of disturbance is equal to the end time minus the beginning time. The stabilization time after releasing the throttle was calculated by subtracting the time that the throttle was released from the ending time of downwash air speed disturbance. The stabilization time after the rotor speeds returned to hover was calculated likewise.

For all tests, including those not shown in Table 4, the time required for the UAV to return to hovering rotor speeds was approximately 5 s after the throttle was released. Overall, the stabilization times ranged from 4 to 11 s (avg. 6 s, std. dev. 1.5 s) after releasing the throttle and from 0 to 6 s (avg. 2 s, std. dev. 1.4 s) after the UAV rotor speeds have returned to hovering speeds. Removing the data from the 0.52 m and 0.88 m readings, which are believed to be in the extremely turbulent portion of the downwash region, does not change the average values, but it does improve the standard deviation to 1.4 s after releasing the throttle and 1.3 s after returning to hovering rotor speeds.

Figure 6 shows all results for the vertical UAV motion. As shown, there is an upward trend in stabilization time as the distance from the UAV increases, though the linear R^2 value is too low to consider the trend line to be statistically significant. All 53 instances of vertical movement produced significant changes in wind speed. During the period of simulated motion, the average deviations were 128% for the rotor speed and 129% for the wind speed. Note that some values actually returned to standard hovering wind speeds prior to the UAV fully reaching hovering speeds. These are the points that required 0 or fewer seconds for the wind speeds to stabilize. 10 out of 53 tests were stabilized by the time the rotor speeds returned to hovering speeds, so 19% of the observed movements did not cause significant downwash disturbance beyond the time that the UAV was in motion.

3.5. Rotational movement

For rotational movement, the operator engaged the throttle for 5 s, reaching peak rotor speeds up to 6.2% greater than the hovering rotor speed. The low changes in rotor speed produced lower changes in air speed, which made determination of the disturbance time less precise. The results for Flight 1, anemometer 2, and Flight 5, anemometer 2, are shown in Table 5, and the results were found using the same methods as with the results in Table 4. The two results in Table 5 were selected because they contain the greatest number of significant disturbances.

For all tests, it took less than 0.25 s for the UAV to return to hovering rotor speeds after releasing the throttle, which is significantly faster than seen in the vertically upwards movement tests, likely due to the significantly slower rotor speeds. Since the anemometer only sampled once per second, the stabilization time was the same after releasing the throttle and after returning to hovering rotor speeds. Another considerable difference with the rotational movement tests is that only 15 out of 45 tests were able to see a significant change in wind speeds, and those that did provide results showed even lower statistical significance than the vertical upward movement results. Overall, the stabilization times ranged from -4 to 6 s (avg. 2 s, std. dev. 2.5 s). Note that a negative stabilization time means the region had statistically stabilized prior to the time that the rotors returned to hovering speeds. Compared with the vertical movement results, the much wider range and greater standard deviation show the unreliability of the results, which is undesirable for predicting concentration changes for gas monitoring.

Despite the limitations in predicting exact stabilization time, rotational movement is actually better suited for gas monitoring than vertical movement due to the greater number of instances in which no stabilization time was recorded. Figure 7 shows all results for the rotational UAV motion. As shown, there appears to be a downward trend in stabilization time as the distance from the UAV increases. At 19.46%, the linear R^2 value is still too low to consider the trend line to be statistically significant, though it is very similar to the 20.78% linear R^2 value seen in the vertical upward movement results. The primary difference from the vertical movement results is that only 15 out of 45 rotational tests produced significant changes in wind speed. During the period of simulated movement, the average deviation from the mean rotor speed was 5.8%, and the average deviation for wind speed was 15.7%. Both of these values are significantly lower than seen in the vertical movement tests,

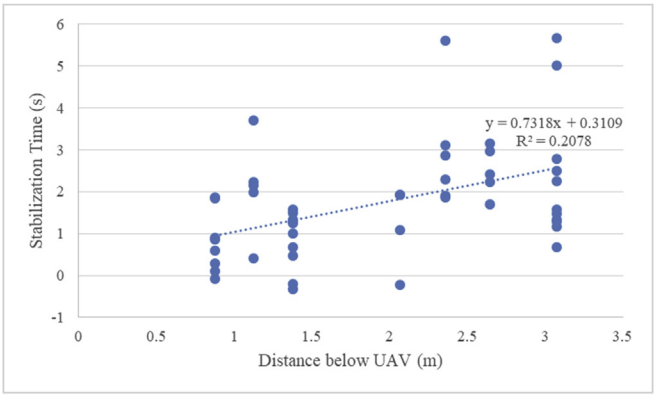

Figure 6. Results for vertical motion stabilization time after returning to hovering rotor speeds.

Table 5. Results after simulating rotational UAV movement, flight 1 & flight 5.

Anemometer Location	No.	Event Times (s)					Time Downwash Air Speed Was Disturbed (s)			Stabilization Time (s)	
		Throttle Applied	Throttle Released	Throttle Duration	Rotor Speeds Return to Hover	Time to Return to Hover	Begin	End	Total	After Releasing Throttle	After Rotor Speed Returns to Hover
2.07 m below the UAV	1	369.386	373.968	4.582	374.071	0.103	-	-	-	-	-
	2	434.054	438.738	4.684	438.772	0.034	434	439	5	0	0
	3	497.888	504.044	6.156	504.112	0.068	500	507	7	3	3
	4	564.444	569.532	5.088	569.598	0.066	570	573	3	3	3
	5	629.580	634.393	4.813	634.426	0.033	635	636	1	2	2
3.48 m below the UAV	1	98.821	103.806	4.582	103.941	0.135	-	-	-	-	-
	2	163.614	168.394	4.684	168.530	0.136	164	165	1	-3	-4
	3	229.081	234.481	6.156	234.619	0.138	231	232	1	-2	-3
	4	359.767	364.659	5.088	364.794	0.135	359	365	6	0	0
	5	424.612	429.867	4.813	429.969	0.102	425	428	3	-2	-2

and the lower rotor speeds are likely the primary reason why most of these tests did not produce significant results. Additionally, 7 of the measured results stopped showing downwash disturbance during UAV motion or immediately when UAV motion ceased, which means only 8 out of 45 rotational tests produced significant changes in wind speed that lasted longer than UAV motion. For this experiment, stabilization time did not matter for 82% of tests, which implies that rotational movement causes a more desirable disturbance for gas monitoring than vertical movement.

3.6. Horizontal movement

For aforementioned reasons, horizontal movement could not be simulated while attached to the stand. However, since horizontal motion does not change potential energy, low changes in rotor speed similar to the rotational movement results can be expected. A flight was performed outdoors to test this prediction, and the weather conditions at the time of the flight were 25 °C, 5 mph wind speed, and 82% humidity. 6 min of data was recorded while the UAV was hovering to obtain the average hovering speed, which was 2842 RPM. Over periods of 3 min, the rotational movement produced a 9% average deviation in rotor speed from the hovering speed, while the horizontal movement produced 4% average deviation. Because the horizontal motion deviation is lower than rotational, it is predicted that horizontal motion will produce even less downwash disturbance time than rotational motion.

4. Conclusions

Downwash region stabilization times were determined after movement was simulated using a 6-rotor UAV. Data was collected by mounting the UAV to a stand, placing the stand in a controlled indoor environment with no external sources of airflow, and placing anemometers at ten locations beneath the UAV. Wind speed results while the UAV was not in motion show a decrease in standard deviation until 2.07 m beneath the UAV rotors, which then remains constant at 2.36 m. Beyond 2.36 m, standard deviation begins increasing, though this is likely due to air backwash as the wind impacts the ground. Such backwash is not expected to be a problem for open air testing, but it may interfere with testing performed indoors or in underground mines and tunnels. Turbulence likely causes higher standard deviations, and low reliability in gas concentrations is linked to turbulence. Therefore, the ideal measuring point for this test's UAV stand is 2.07–2.36 m below the UAV rotors because this range of distances experienced the least turbulence. Without ground interference, the authors believe the turbulence will continue decreasing beyond 2.07 m below the UAV rotors, though this hypothesis remains untested. Additionally, wind speeds proved extremely turbulent at 0.52 m and 0.88 m, but not at 1.13 m. Papers by other authors have discussed a conical region of low wind speed beneath the body of the UAV. This experiment's results show that the conical region extends to a point 0.88–1.13 m beneath the rotors for the UAV used for this project. Samples taken within this region experienced considerably higher turbulence, which implies that gas samples should not be collected in the conical region of any UAV. Future tests with this UAV should place the measuring point at least 1.13 m from the UAV rotors, or closer if the conical region is better defined.

The wind speed results with UAV movement found that stabilization times after vertical upward UAV motion ranged from 4 to 11 s (average of 6 s) after releasing the throttle, or 0–6 s (average of 2 s) after the rotor speeds returned to the average hovering speeds. The average values had a standard deviation of 1.4 s and 1.3 s, respectively, which are both lower than the 2.5 s standard deviation seen in stabilization times after rotational movement. Stabilization times after rotational UAV motion ranged from -4 to 6 s after the rotor speeds returned to the average hovering speeds. The significantly lower air speeds measured during rotational UAV movement likely caused the greater deviation. The low air speeds were a result of the significantly lower rotor speeds. The wind speed was so low that only 18% of tests produced significant wind disturbance that lasted longer than the period of UAV motion, whereas this value for vertical motion is 81%. Therefore, it can be concluded that rotational UAV movement during gas monitoring is more desirable than vertical movement because the rotational movement is much less likely to alter the downwash region significantly. However, both types of motion can still cause downwash disturbance up to 6 s after UAV motion has ceased, which means it is desirable to avoid any motion during gas sampling. Some evidence suggests that horizontal motion may be even less likely to produce downwash disturbance that lasts longer than the period of UAV motion, though this project was not able to collect wind speed data to verify this hypothesis.

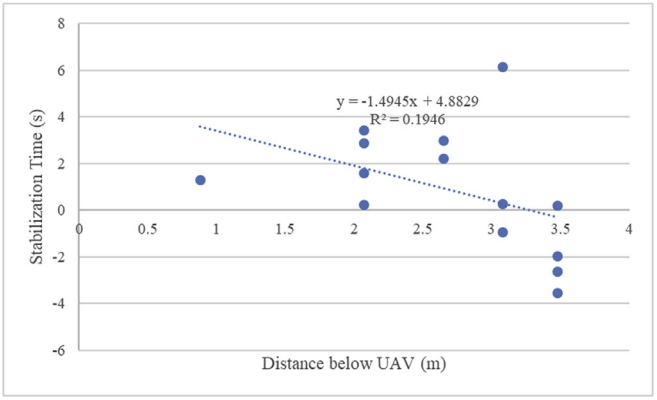

Figure 7. Results for Rotational Motion Stabilization Time after Returning to Hovering Rotor Speeds (Note: Negative times indicate the wind speed is stable before UAV motion has ceased).

5. Future works

To obtain results for vertically downward motion and to gain more insight regarding horizontal motion, a building or other structure may be found that will both prevent wind and GNSS interference, which would negate the necessity for the UAV stand. More testing must be performed to determine the distance from the ground at which backwash will affect results. Additional testing can also be used to better define the extremely turbulent region immediately beneath the UAV, which likely ends between 0.88 and 1.13 m beneath the UAV rotors. An anemometer with a higher sampling rate could result in more accurate stabilization time results, though such an anemometer was not commercially available at the time of this project. One option for improving the downwash region definition could be the use of improved anemometer technology that is capable of higher sampling rates and improved wind direction definition, such as 2D/3D ultrasonic anemometers. A validated computational fluid dynamics simulation to compare experimental work to could also be developed to remove interference from a stand or building but computation time would be very large for a direct comparison to the work presented in this manuscript.

Declarations

Author contribution statement

Jacob L. Brinkman: Conceived and designed the experiments; Performed the experiments; Analyzed and interpreted the data; Contributed reagents, materials, analysis tools or data; Wrote the paper.

Brent Davis: Performed the experiments; Analyzed and interpreted the data.

Catherine E. Johnson: Conceived and designed the experiments; Analyzed and interpreted the data; Wrote the paper.

Funding statement

This work was supported by the Society of Mining, Metallurgy and Exploration.

Competing interest statement

The authors declare no conflict of interest.

Additional information

No additional information is available for this paper.

Acknowledgements

Thanks to research technicians Jeff Heniff and Fred Eickelmann for designing and building the UAV stand. Thanks also to fellow graduate students Kelly Williams, Barbara Rutter, Martin Langenderfer, and David Doucet for assisting with some or all of the tests. Funding for this work was from the SME 2017 Freeport McMoRan Career Development Grant Program (PI: Dr. Catherine Johnson, Award Number 00057881).

References

Aboubakr, Mohamed, Ahmed, Balkis, Ali-Abou, ElNour, Tarique, Mohammed, 2017. Environmental Monitoring System by Using Unmanned Aerial Vehicle, 9. *Network Protocols and Algorithms*.

Ali, Henok, Odeh, Momen, Ahmed, Odeh, Abou El-Nour, Ali, Tarique, Mohammed, 2017. Unmanned Aerial Vehicular System for Greenhouse Gas Measurement and Automatic Landing, 9. *Network Protocols and Algorithms*.

Alvear, Oscar, Roberto Zema, Nicola, Natalizio, Enrico, Carlos, T., Calafate, 2017. Using UAV-based systems to monitor air pollution in areas with poor accessibility. J. Adv. Transport. 2017.

Alvear, Oscar, Calafate, Carlos T., Zema, Nicola Roberto, Natalizio, Enrico, Hernandez-Orallo, Enrique, Cano, Juan-Carlos, Manzoni, Pietro, 2018. A discretized approach to air pollution monitoring using UAV-based sensing. Mob. Netw. Appl. 23.

Alvarado, Miguel, Gonzalez, Felipe, Erskine, Peter, Cliff, David, Heuff, Darlene, 2017. A methodology to monitor airborne PM10 dust particles using a small unmanned aerial vehicle. Sensors 17.

Aurell, J., Mitchell, W., Chirayath, V., Jonsson, J., Tabor, D., Gullett, B., 2017. Field determination of multipollutant. Jul 28. In: Open Area Combustion Source Emission Factors with a Hexacopter Unmanned Aerial Vehicle, 166. *Atmospheric Environment*.

Barchyn, Thomas E., Hugenholtz, Chris H., Myshak, Stephen, Bauer, Jim, 2018. A UAV-based system for detecting natural gas leaks. J. Unmanned Veh. Syst. 6 (1).

Bolla, Gian Marco, Casagrande, Marco, Comazzetto, Antonio, Dal Moro, Riccardo, Destro, Matteo, Fantin, Edoardo, Colombatti, Giacomo, Aboudan, Alessio, Enrico, C., Lorenzini, 2018. ARIA: air pollutants monitoring using UAVs. In: Proceedings of the 2018 5th IEEE International Workshop on Metrology for Aerospace. IEEE.

Brady, James M., Dale Stokes, M., Jim Bonnardel, Timothy, H. Bertram., 2016. Characterization of a quadrotor unmanned aircraft system for aerosol-particle-concentration measurements. Environ. Sci. Technol. 50. Jan 5.

Chang, Chih-Chung, Wang, Jia-Lin, Chang, Chih-Yuan, Liang, Mao-Chang, Lin, Ming-Ren, 2016. Development of a multicopter-carried whole air sampling apparatus and its applications in environmental studies. Chemosphere 144.

Chang, Chih-Chung, Chang, Chih-Yuan, Wang, Jia-Lin, Lin, Ming-Ren, Ou-Yang, Chang-Feng, Pan, Hsiang-Hsu, Chen, Yen-Chen, 2018. A study of atmospheric mixing of trace gases by aerial sampling with a multi-rotor drone. Chemosphere 144.

DJI (Dà-Jiāng Innovations Science and Technology Co., Ltd), 2018. Matrice 600 Pro: Specs. DJI.

Gu, Qijun, Michanowicz, Drew R., Jia, Chunrong, 2018. Developing a modular unmanned aerial vehicle (UAV) platform for air pollution profiling. Sensors 18.

Haas, Patrick, Balistreri, Christophe, Pontelandolfo, Piero, Triscone, Gilles, Pekoz, Hasret, Pignatiello, Antonio, 2014. Development of an unmanned aerial vehicle UAV for air quality measurements in urban areas. Jun. In: Proceedings of the 32nd American Institute of Aeronautics and Astronautics (AIAA) Applied Aerodynamics Conference. AIAA. iljujjkin. Sep 27, 2017. "DJI Matrice 600 Pro 2017 Model.TurboSquid.

Liu, Fan, Zheng, Xiaohong, Qian, Hua, 2018. Comparison of particle concentration vertical profiles between downtown and urban forest park in nanjing (China). Atmos. Pollut. Res. 9.

McCray, Robert B., 2016. Utilization of a small unmanned aircraft system for direct sampling of nitrogen oxides produced by full-scale surface mine blasting. In: Theses and Dissertations – Mining Engineering. University of Kentucky.

Nash, Susan Smith. Jan, 2017. Drones and UAVs for methane emissions detection, monitoring, and regulatory compliance. IJRDO J. Biol. Sci. 3 (1).

Neumann, Patrick P., 2013. Gas Source Localization and Gas Distribution Mapping with a Micro-Drone. Masters Thesis.

Ni, Jun, Yao, Lili, Zheng, Jingchao, Cao, Weixing, Zhu, Yan, Tai, Xiuxiang, 2017. Development of an unmanned aerial vehicle-borne crop-growth monitoring system. Sensors 17.

Qing, Tang, Zhang, Ruirui, Chen, Liping, Xu, Min, Yi, Tongchuan, Zhang, Bin, May, 2017. Droplets movement and deposition of an eight-rotor agricultural UAV in downwash flow field. Int. J. Agric. Biol. Eng. 10 (3).

Roldan, Juan Jesus, Joossen, Guillaume, David, Sanz, del Cerro, Jaime, Barrientos, Antonio, 2, 2015. Mini-UAV based sensory system for measuring environmental variables in greenhouses. Sensors 15 (Feb).

Shukla, Dhwanil, Narayanan, Komerath, 2018. Multirotor drone aerodynamic interaction investigation. Drones 2.

Smidl, Vaclav, Hofman, Radek, 2013. Tracking of Atmospheric Release of Pollution Using Unmanned Aerial Vehicles, 67. *Atmospheric Environment*.

Villa, Tommaso Francesco, Salimi, Farhad, Morton, Kye, Morawska, Lidia, Gonzalez, L. Filipe, 2016. Development and validation of a UAV based system for air pollution measurements. Sensors 16 (2202).

Villa, Tommaso Francesco, Jayaratne, E. Rohan, Gonzalez, L. Filipe, Morawska, Lidia, 2017. Determination of the vertical profile of particle number concentration adjacent to a motorway using an unmanned aerial vehicle. Environ. Pollut. 230 (Nov).

Villa, Tommaso Francesco, Brown, A. Reece, Jayaratne, E. Rohan, Gonzalez, L. Felipe, Lidia, Morawska, Ristovski, Zoran D., 2019. Characterization of the particle emission from a ship operating at sea using an unmanned aerial vehicle. Atmos. Meas. Tech. 12 (1) (Jan).

Yang, Fengbo, Xue, Xinyu, Zhang, Ling, Sun, Zhu, 2017. Numerical simulation and experimental verification on downwash air flow of six-rotor agricultural unmanned aerial vehicle in hover. Int. J. Agric. Biol. Eng. 10 (4).

Yang, Fengbo, Xue, Xinyu, Cai, Chen, Sun, Zhu, Zhou, Qingqing, 2018. Numerical simulation and analysis on spray drift movement of multirotor plant protection unmanned aerial vehicle. Energies 11.

Yao, Yao, Wei, Shanlin, Zhang, Honghui, Li, Qiong, 2018. Application of UAV in monitoring chemical pollutant gases. Chemical Eng. Trans. 67.

Yeo, Derrick, Shrestha, Elena, Paley, Derek A., Atkins, Ella, 2015. An empirical model of rotorcraft UAV downwash model for disturbance localization and avoidance. In: Proceedings of the American Institute of Aeronautics and Astronautics (AIAA) Atmospheric Flight Mechanics Conference, 2015. AIAA.

Zheng, Yongjun, Yang, Shenghui, Liu, Xingxing, Wang, Jie, Norton, Tomas, Chen, Jian, Tan, Yu, 2018. The computational fluid dynamic modeling of downwash flow field for a six-rotor UAV. Front. Agri. Sci. Eng. 5 (Issue 2).

Zhou, Xiaochi, Aurell, Johanna, Mitchell, William, Tabor, Dennis, Gullett, Brian, 2017. A small, lightweight multipollutant sensor system for ground-mobile and aerial emission sampling from open area sources. Atmos. Environ. 154.